

# PROBABILISTIC PRINCIPAL COMPONENT AND LINEAR DISCRIMINANT ANALYSIS OF INTERACTION OF 1064 NM CW LASER WITH ICP PLASMA: WHISTLER WAVE EXITED ANTI STOKES COOLING

M.F. Yilmaz<sup>1</sup>, H.U. Rahman<sup>2</sup>, F. Paletou<sup>3</sup>, F Yilmaz<sup>4</sup> T. Malas<sup>5</sup>, B. Karlik<sup>6</sup>

<sup>1</sup>Independent Researcher, Fremont, CA, USA

<sup>2</sup> Magneto-Inertial Fusion Technology, Inc., Tustin, CA, USA

<sup>3</sup>Université de Toulouse, Observatoire Midi-Pyrénées, CNRS, CNES, IRAP, F-31400 Toulouse, FRANCE

<sup>4</sup>Department of Computer Sciences, New Jersey Institute of Technology, New Jersey, NY, USA

<sup>5</sup>Lorentz Solution Inc, Fremont, CA, USA

<sup>6</sup> Neurosurgical Simulation Research and Training Centre, Department of Neurosurgery, Montreal Neurological Institute and Hospital, McGill University, CANADA

## ABSTRACT

Pattern recognition techniques are known to play an emerging role for studying underlying physics of light-matter interaction. Photon condensation and Anti-Stokes cooling remain compelling phenomena of laser plasma interaction. In this work, the interaction of a 1064 nm continuum-wave laser with inductively-coupled plasma (ICP) of Hg has been studied by probabilistic pattern recognition over observed time resolved spectral data. Probabilistic principal component analysis (PPCA) over spectral data reveals the collective behavior of condensation and Stokes and Anti-Stokes line profiles. Probabilistic linear discriminant analysis (PLDA) of spectra proficiently illuminates the homoclinic orbit Whistler waves in 3D and decompose the spectral data to up and down scattered photons spectra as well as phonon-electron(hybrid) spectrum. According to hybrid spectrum, cooling is maintained by the electron-phonon relaxation. On the other hand, electron oscillation ( $\omega_{pe} = 0.16$  kHz) and density ( $n_e \sim 4 \times 10^{13}$  cm<sup>-3</sup>) of plasma are extracted by PLDA which does not demand kinetic modeling of spectra.

## INTRODUCTION

Plasmas are tunable mediums, which, in turn, can act as absorbers, transmitters or reflectors, depending on the frequency range and application of interest. Therefore, plasmas are known to have a widespread use in industry for several applications, such as stealth technologies in radar applications and radio communications. In this context, the propagation of radio-frequency (RF) electromagnetic waves in uniform, non-uniform, magnetized or unmagnetized plasmas have been studied extensively both experimentally and theoretically [1]–[4]. It has been shown that it is possible to obtain high levels of absorption in a broadband range including RF and microwave frequencies [5]–[7] by adjusting some plasma parameters, such as magnetic field strength and plasma density. However, the propagation of low-intensity laser light within cold plasmas have found less interest in comparison to RF or microwave

electromagnetic waves emitted from antennas [4], [8]–[10]. Although laser is indeed a special form of electromagnetic wave with extremely high frequency and propagation of laser can be best described by the wave model, a plausible explanation of the absorption mechanism needs the particle model. For instance, the Drude model elucidating the interaction of RF waves within plasma has failed to explain the loss mechanism of plasma after the introduction of a laser beam [8]. Besides, laser cooling of nanoparticles and semiconductors has been studied in detail and most of the studies suggest the cooling is attributed to photon up conversion mechanisms and anti-Stokes shifting, especially for room temperature mediums [10 and 11].

In this study, we investigate the radiation loss of plasma by means of Stokes and Anti-Stokes polarization of photons in ICP Mercury plasma that is revealed by probabilistic pattern recognition techniques over time resolved spectra. Principal component analysis (PCA) and linear discriminant analysis (LDA) are well-known pattern recognition methods for processing and carrying out dimension reduction of the data. PCA and LDA have found application in several areas, such as medicine, robotics and remote sensing. They have also been found in many applications in spectroscopy, especially in unmixing species and decomposing overlapped spectral lines of UV-VIS-NIR spectroscopy to extract the spectral fingerprints. In addition, they are used in the spectroscopy of astrophysical plasmas and laboratory plasmas for extracting the plasma parameters and compositions of ion species [12]–[18]. While PCA does identify the linear subspace in which most of the data's energy is concentrated, LDA identifies the subspace wherein data between different classes is most spread out. This, in turn, makes LDA suitable for recognition problems such as classification. In the meantime, PCA and LDA have limitations related to dimensionality reduction, such as nonparametric representation of data and high computational cost. Tipping et al. 1999 and Ioffe et al. 2006 [19 and 20] posited that the probabilistic model can represent the data with few parameters and reduce to dimensions using Gaussian Density model in order to manage the computation time.

In this study, the interaction of continuum mode 1064 nm diode laser light with the ICP Mercury plasma is analyzed both experimentally and theoretically. The experimental part is premised on the power-meter measurements and spectroscopy. PPCA and PLDA over UV-Vis spectra of Hg plasma is used as a feature extractor to investigate the polarization, scattering structures and electron temperature, as well as density of the plasma in the presence of different powers of laser beam. Similarly, the theoretical component is premised on the study of the PPCA and PLDA analysis and non-local thermal equilibrium (non-LTE) radiative modeling of experimental spectra both in the absence and presence of laser beam.

## METHODS

### Experiment

The uniform magnetized plasma slab has been generated by inductively coupling a 13.56 MHz RF generator (60 Watts) to the fluorescent light bulb, which has a length of 30 cm and a diameter of 2.0 cm.

The spectra have been recorded by a charge-coupled (CCD) spectrometer device of AvaSpec-ULS3648. Continuum-wave (CW) diode laser lights at different powers was directed to the plasma, after which power levels were recorded by means of a Thorlab-PM100D power-meter. Fig. 1a illustrates the laser powers and corresponding absorbance coefficients that are obtained using standard loss medium model. It can be seen that low power laser attenuated quickly, and that the plasma becomes transparent to the laser beam as the power of laser increases. Fig. 1b shows the experimental spectra of mercury plasma in the absence and presence of laser light at different powers.

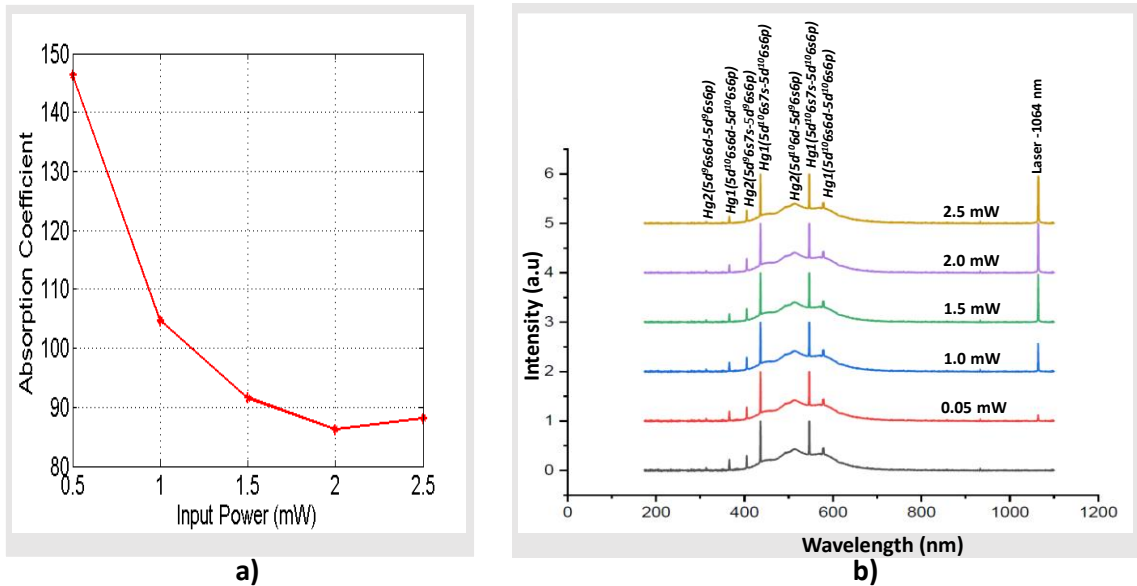


Fig. 1 a) Absorption coefficients at different laser powers and b) UV and UV-Vis spectra of Mercury plasma in the absence and the presence of the laser light.

### Probabilistic principal component and linear discriminant analysis

The main objective of Principal Components Analysis (PCA) is applying linear transformation techniques to extract the maximum variance from the data set with each component. Due to the nature of the model selection criteria and information complexity criterion, the most important requirement of applying an information criterion for a model is the existence of a maximum likelihood estimator. However, classical principal component analysis lacks a probability model that is necessary to derive maximum likelihood estimation. Tipping and Bishop have proposed that in a latent variable model closely related to factor analysis, the maximum likelihood estimation of the parameters could be used to construct the fundamental axes of a set of observed data vectors named as the Probabilistic Principal Component Analysis (PPCA). Notably, PPCA is the probabilistic version of the well-known PCA method. It is based on a Gaussian-latent variable model related to Bayesian statistical factor analysis. Gaussian-latent variable model utilizes the transformation  $t = Wx + \mu + \varepsilon$ , where  $d \times q$  matrix  $W$  relates the  $d$ -dimensional observation vector  $t$  corresponding  $q$  dimensional vector of the unobserved variable

x. The parameter vector  $\mu$  maintains the observation vector to have non-zero values capable of performing in the presence of missing values in the data [19].

Linear Discriminant Analysis (LDA) distinguishes the data in the data set in accordance with the properties of the data when it is assigned to variable groups. The discriminant functions obtained through discriminant analysis consist of linear components of estimation variables. LDA confronts challenges when the discriminative information is not in the means of classes and small sample size problem. PLDA model is the probabilistic version of LDA wherein both inter-class and in-class variances are represented as multidimensional Gaussians. As a matter of fact, the relationship between PCDA and PLDA is analogous to that of between factor analysis and principal components analysis. It is possible to build a model of a previously unseen class using a single example with PLDA. Moreover, it is easy to combine multiple examples for a better representation of the class. Let us assume that data base consists of  $J$  observations corresponding to each  $I$  members. The  $j$ 'th information of the  $i$ 'th individual is denoted by  $X_{ij}$ . The model uses the process of  $X_{ij} = \mu + Fh_i + Gw_{ij} + \varepsilon_{ij}$  for data generation of the signal component  $\mu + Fh_i$  and the noise component  $Gw_{ij} + \varepsilon_{ij}$  of the database. Similarly, the matrix  $F$  and  $G$  correspondingly provide bases between-individual subspace and within-individual subspace. The term  $\mu$  represents the arithmetic mean of the dataset. Gaussian residual noise  $\varepsilon_{ij}$  with diagonal covariance  $\Sigma$  represents the unexplained data. Signal component of data depends only on the identity of members and noise term is different for each information of the member, representing within-individual noise. More detailed explanation can be found in studies conducted by Tipping et al., 1999, Ioffe et al., 2006 and Prince et al., 2007 [19 and 20].

In the present work, PCA is applied to the set of 60 spectra of size 2831x1 for the laser powers of 0.0, 0.05, 1.0, 1.5, 2.0 and 2.5 mW. Principal components are eigenvectors of the covariance matrix consisting of the covariances between different variables and hence, is a matrix of size 2831x2831. Therefore, each vector (principal component) also has a size of 2831x1. Then original data is projected onto the space spanned by the first three, most dominant, principal components denoted by  $|PC1\rangle$ ,  $|PC2\rangle$  and  $|PC3\rangle$ . As the first step, PCA is used to reduce the size of within-class scatter matrix ( $S_w$ ) for each electron beam fraction so that it can be inverted. The data set comprises of 6 laser powers (0.0, 0.05, 1.0, 1.5, 2.0 and 2.5 mW)  $\times$  60 spectra of size  $2831 \times 1$ . By applying PPCA, the dimension is reduced to 30 by projecting each of the spectra into the space generated by the most dominant 30 PCs. As the second step, PLDA is applied to the 6 classes of powers where each class consists of 360 vector of size  $2831 \times 1$ , with the dimension being reduced to 3. The new vector space is generated by  $|LD1\rangle$ ,  $|LD2\rangle$  and  $|LD3\rangle$ .

## RESULTS

3D plots of PC1, PC2 and PC3 coefficients are illustrated in Fig. 2, which demonstrate that the increase of laser power causes the plasma to be more collective and linearizes except for the 0.5 mW of laser

power.  $|\text{PC1}\rangle$  vector spectra in Fig. 3a correspond to the polarization due to E-field of laser, whereas Fig. 3b is the zoom out of  $|\text{PC1}\rangle$  vector spectra. This shows the enhancement of intensities (Stokes I polarization profiles) by increasing the laser power.  $|\text{PC2}\rangle$  vector spectra in Fig. 4a correspond the polarization due to B-field of the laser and Hg1 ( $5d^{10}6s7s-5d^{10}6s6p$ ) line follows the circular polarization profiles of Stokes V. Furthermore, Fig. 4b illustrates the zoom out of spectral line of Hg2, while the peak of the line of Hg2 experiences the Anti-Stokes shifting by increasing the laser power [21 and 22].

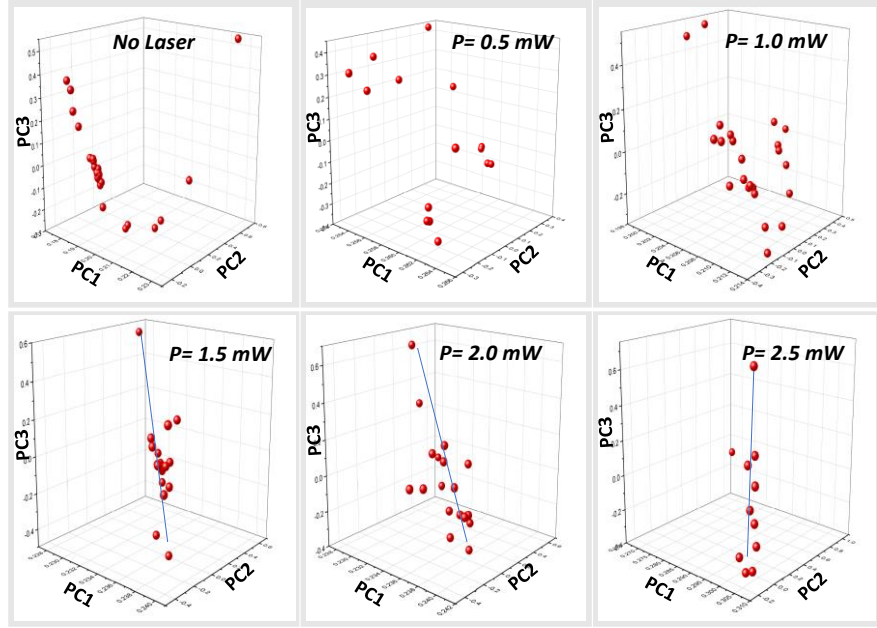


Fig. 2 3D representations of PC of coefficients with increasing laser power.

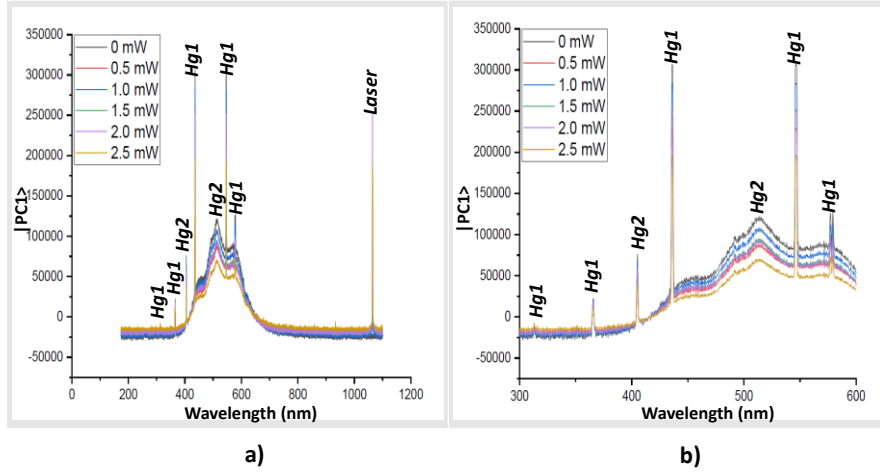


Fig. 3 a)  $|\text{PC1}\rangle$  vector spectra of Mercury with increasing laser power. b) Zoom out of  $|\text{PC1}\rangle$  spectra for 300nm to 600nm range.

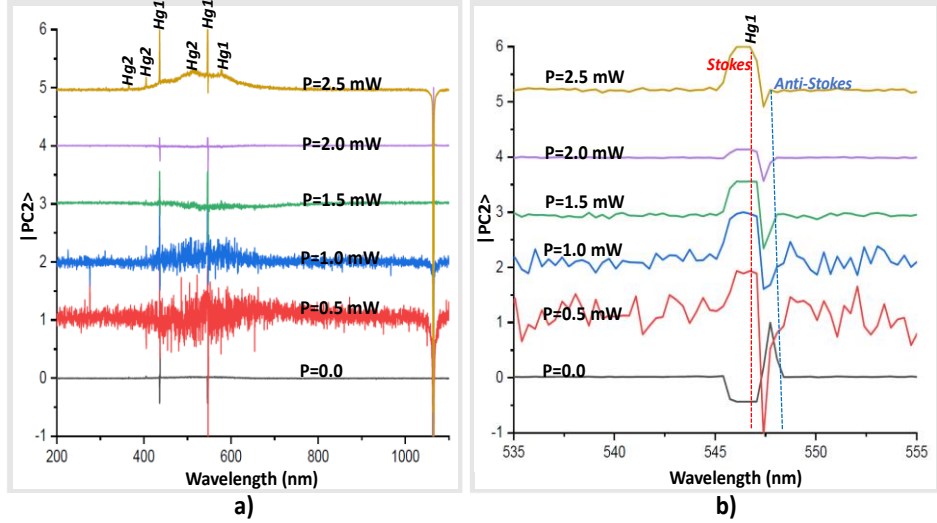


Fig. 4 a)  $|\text{PC2}\rangle$  vector spectra of Mercury plasma in the absence and presence of laser beam with different powers. b) Zoom out of  $|\text{PC2}\rangle$  spectra.

Plasma electron temperature modeling of experimental spectra is realized by SPARTAN radiative transfer code. SPARTAN uses the non-thermal plasmas approach that follows the thermal equilibrium and velocity distributions of ions as well as non-Maxwellian distributions of electrons [23]. SPARTAN generated synthetic spectra in Fig. 5a demonstrates that the intensity of all considered transitions with an increase in the plasma electron temperature in the absence of laser power modeled ( $\text{Te}=0.85 \text{ eV}$ ). Besides, it is possible to use Anti-Stokes—Stokes intensity ratios to observe the trends of plasma electron temperature [22]. For that reason, we have used the Anti-Stokes—Stokes intensity ratios of transition of  $\text{HgI}(5d^{10}6s7s-5d^{10}6s6p)$  at 546 nm to obtain the trends of electron temperatures with the corresponding laser powers (Fig.4b) Fig. 5b shows that plasma is only heated to 7 eV by the 0.5 mW of laser power than cooled by the increasing the laser power.

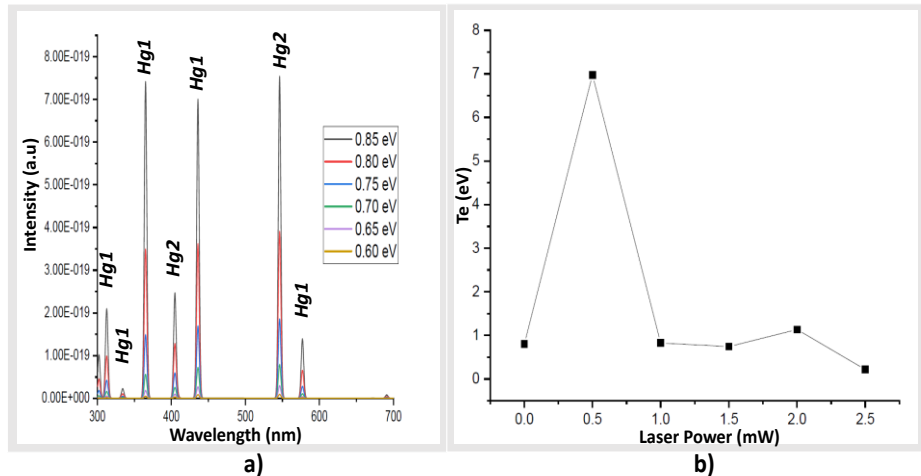


Fig. 5. a) Plasma electron temperature dependence of non-LTE synthetic spectra at electron density of  $1 \times 10^{13} \text{ cm}^{-3}$  b) Modeling of plasma electron temperature with corresponding laser power.

3D representation of PLDA has been illustrated in Fig.6a. As shown in the figure, photons are up and down scattered to the form of Whistler wave mode.  $|LD1\rangle$ ,  $|LD2\rangle$  and  $|LD3\rangle$  vector spectra are illustrated in Fig. 6b.  $|LD1\rangle$ ,  $|LD2\rangle$  and  $|L3\rangle$  correspondingly denote down scattered, up scattered and electron-phonon coupling spectrum. Down shifted spectrum has higher intensities and electron-phonon spectrum has relatively lower intensities [25]. Zoom out of electron-phonon spectrum has been illustrated in Fig.6c. with the presence of the absorptions of Hg1 at 437 nm and 546 nm. Electron oscillations spectrum ( $|LD4\rangle$ ) are represented in Fig. 6d. Modeling of electron oscillations using Fourier series suggests that the electron oscillations is around 166 Hz (0.16 kHz). The plasma electron density ( $n_e \sim 4 \times 10^{13} \text{ cm}^{-3}$ ) is obtained using the Eq.1, where  $\omega_{pe}$  denotes the electron frequency and  $\epsilon_0$  signifies the permittivity of the free space [26 and 27]

$$\omega_{pe} = \sqrt{n_e e^2 / \epsilon_0 m_e} \quad (1)$$

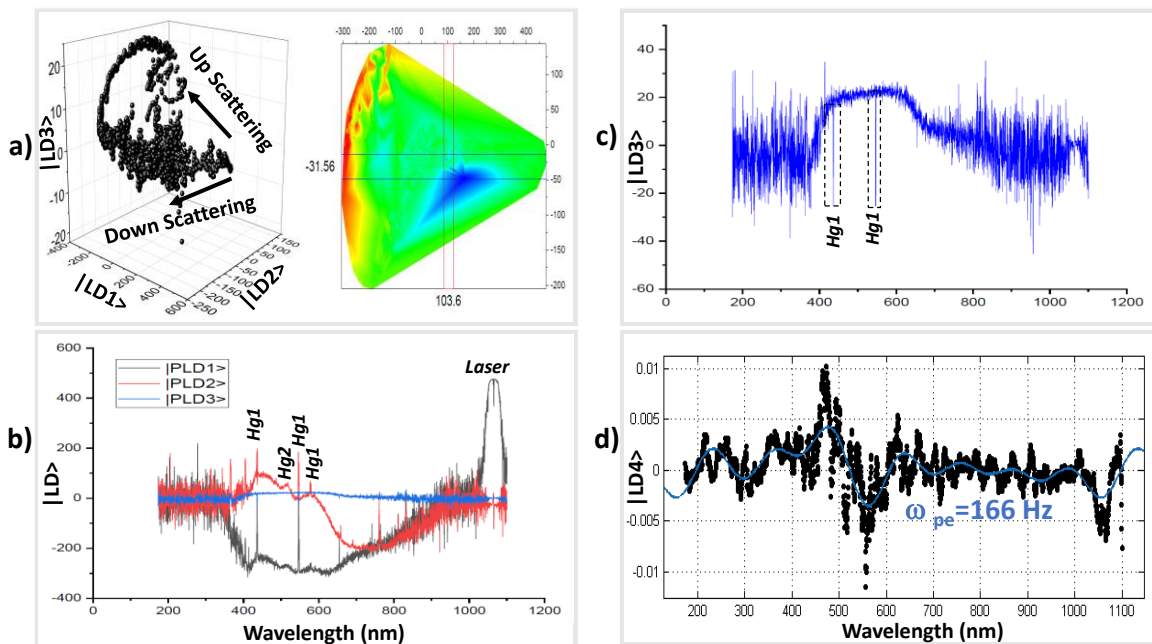


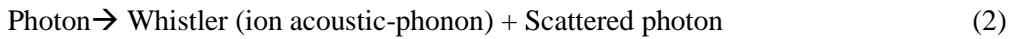
Fig. 6 a) 3D representation of PLD coefficients with topological view b) Up scattered( $|LD1\rangle$ ), down scattered( $|LD2\rangle$ ) photon, phonon( $|LD3\rangle$ ) vector spectra of Mercury plasma. c) zoom out of electron-phonon spectrum d) electron ( $|LD4\rangle$ ) spectrum and its FFT modeling.

## DISCUSSION

Laser light can cool, trap and condensate the atoms/molecules. Leduc et al.2009 stated that when particles are condensate by the laser or magnetic cooling, interparticle distance become smaller and particles follows the collective behavior [28]. Plasma condensation is usually pronounced in coronal plasmas and realized when magnetic force dominates the gravitational and the pressure forces [29]. Recently, the enhancement of the intensity of radiation and strong electric fields in coronal loops, has been depicted by the stability of the plasma condensation [30]. Collective behavior of plasma associated

with the cooling of electron temperatures in our data agrees with the fact that plasma is condensate by the increase of laser power with the exception of 0.5 mW.

Light propagates in plasma medium following the dispersion relation  $\omega^2 = \omega_{pe}^2 / \langle \gamma \rangle + k^2 c^2$ , where  $\omega$  signifies the frequency of light,  $\omega_{pe} = \sqrt{n \epsilon_e e^2 / \epsilon_0 m_e}$  shows the plasma frequency and the average  $\langle \gamma \rangle$ -factor. For lasers  $\omega \gg \omega_{pe}$  holds in general, and the wave number becomes almost identical to that of the free space [27]. This amounts to no reflection at the boundaries and scattering, thus causing loss of energy. Stimulated Brillouin scattering of intense laser radiation in plasma is one of the most important parametric process, which describes the decay of the incident laser radiation into the scattered electromagnetic wave as well as an ion acoustic wave-phonon (Eq.2).



Down and up scattered spectra and phonon spectrum illustrated in Fig. 6.a shows that the scattered photons are downshifted (Stokes,  $\omega - \ell h$ ,  $k_-$ ) and upshifted (anti-Stokes,  $\omega + \ell h$ ,  $k_+$ ) by the plasma to finally form Whistler waves. Whistler waves have been observed in under dense plasmas with very low frequency propagation along a magnetic field  $B$ . It is circularly polarized and occurs when plasma frequency is less than that of the electron cyclotron frequency. The interaction between whistler waves and lower hybrid waves in a plasma are still among the compelling phenomena. Whistler waves are capable of destabilizing a magnetized plasma by exciting the lower hybrid wave together with the ion acoustic wave (phonon). This excitation is parametric and follows cooling by the energy loss transferred from resonant to non-resonant wave [30, 31 and 32]. Finally, these non-resonant waves conclude to chaotic wave amplitudes. Besides, Rabinovich describes the Whistler waves as homoclinic chaotic strange attractor generated by bifurcation in which a periodic orbit collides with the saddle equilibrium point (resonant) to itself [33, 34 and 35].

The attenuation of laser intensity  $I$  can be modeled by  $\frac{dI}{dx} = -\kappa_{ib} I$ , where  $\kappa_{ib}$  is the inverse bremsstrahlung absorption coefficient. If we denote  $\rho_c$  as the mass density of the plasma corresponding to the critical density, absorption coefficient is shown to scale as follows:

$$\kappa_{ib} \propto \left( \frac{\rho}{\rho_c} \right)^2 Z \lambda^{-2} T_e^{-3/2} \left( 1 - \frac{\rho}{\rho_c} \right)^{-1/2}.$$

Fig. 7.a shows the absorption coefficient versus  $T_e^{-3/2}$  which follows the almost inverse trend shown in Fig. 1. The absorption coefficients obtained in Fig.1 by power measurements reveal that there is a significant absorption in the plasma with the laser power of 0.5 mW and decrease exponentially by increased laser power [36]. Fig.8b shows the resonance of E and B field of the laser light at 0.5 mW obtained by PC vector spectra. This confirms the fact that the plasma's heating is provided by the resonant absorption. Resonance absorption observed when a p-polarized light shine on a plasma with

density gradient ( $\omega=\omega_{pe}$ ) in which polarized light resonantly excites an electron plasma wave at critical density. Further increasing laser power results cooling of the plasma. Fig. 4b illustrates that such cooling is caused by Anti-stokes shifts which can be excited parametrically by the Whistler-mode waves. For the reference, it was shown that circularly driven EM (R-H and L-H) waves can decay into whistler wave and a Langmuir sideband emission. The Langmuir sideband emission has been illustrated as an anti-Stokes (i.e., frequency upshifted) [37 and 38], Anti-Stokes shift is the optical process whereby photons at low energy levels are absorbed and converted to emit at higher energy levels. The extra energy is provided by the dissipation of thermal energy from the medium. Such dissipations can be acquired by multi-photon absorption, Auger recombination and phonon absorption [39]. Fig. 6c illustrates the presence of electron absorption of Hg1 in the phonon spectrum which confirms the electron-phonon coupling. Electron-phonon coupling is the main process that causes heat to flow from the hotter plasma to the phonons [40].

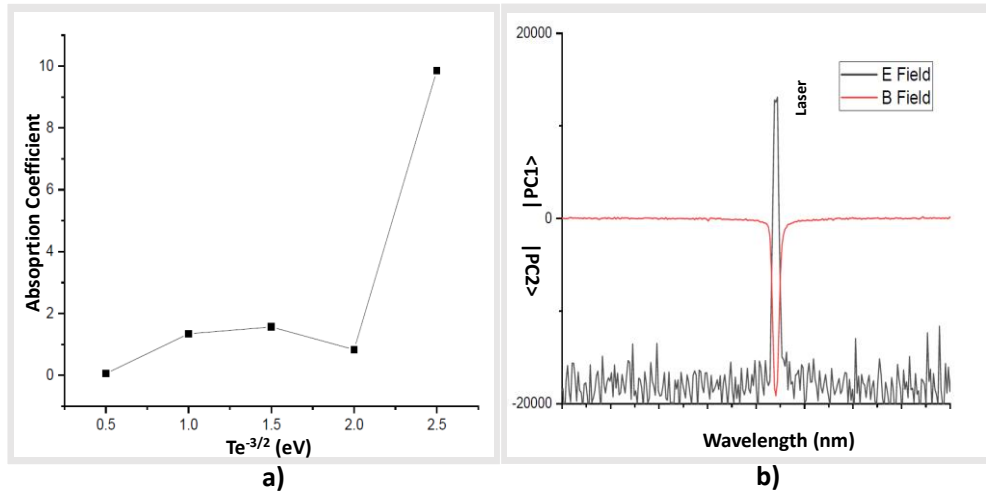


Fig. 7. a) Absorption scaling of laser plasma interaction at different power levels. b) E and B field spectrum of laser spectra at 0.5 mW obtained by PC vectors

## CONCLUSION

In this study, CW laser propagation in cold magnetized collision-less plasma has been investigated by means of probabilistic pattern recognition over emission spectroscopy. PPCA and PLDA over spectra can be used as the non-invasive diagnostic tools of low temperature plasmas. PPCA and PLDA over spectra can distinct the polarization effects due to E and B fields and segregate the upshifted and down shifted spectra and phonon-electron(hybrid) spectrum, correspondingly. Circular polarization is driven through the radiation channels of Hg1 at 536 nm and 546 nm which are mediated by phonons. The spectroscopic modeling of plasma suggests that electron temperature is 0.85 eV and electron density be  $4 \times 10^{13} \text{ cm}^{-3}$  in the absence of laser light, and the temperature is increased to  $\sim 7 \text{ eV}$  at 0.5 mW of laser power due to resonant absorption. However, increased laser power cools the plasma, but more

collective is indicative of plasma condensation. Pattern recognition over the spectra reveals that Whistler Scattering (phonon) assisted Anti-stokes shifting is the main mechanism of the cooling.

#### ACKNOWLEDGEMENTS

This research was funded by The Scientific and Technological Research Council of Turkey (Tubitak-EEAG-113E097).

#### LIST OF REFERENCES

- [1] Jin F., Tong H., Shi Z., Tang D., and Chu P. K, Effects of external magnetic field on propagation of electromagnetic wave in uniform magnetized plasma slabs. *Computer physics communications*, 175, 8, pp.545-552. (2006).
- [2] Tang D. L., Sun A. P., Qiu X. M., and Chu P. K., “Interaction of electromagnetic waves with a magnetized nonuniform plasma slab,” *IEEE Transactions Plasma Science*, 313, pp. 405–410. (2003)
- [3] Sheffield J., Froula D., Glenzer S. H., and Luhmann Jr N. C., *Plasma scattering of electromagnetic radiation: theory and measurement techniques*. Academic Press (2010).
- [4] Kruer W. L., *The physics of laser plasma interactions*. Boulder, Colorado [u.a.] Westview. (2003)
- [5] Vidmar R. J., “On the use of atmospheric pressure plasmas as electromagnetic reflectors and absorbers”, *IEEE Transactions Plasma Science*, 18, 4, pp. 733–741. (1990)
- [6] Aydin K., Ferry, V. E., Briggs R. M., and Atwater H. A., Broadband polarization-independent resonant light absorption using ultrathin plasmonic super absorbers, *Nature Communication.*, 2, 517. (2011).
- [7] Yuan C.X., Zhou Z.X., Zhang J. W., Xiang X.L., Feng Y., and Sun H.G., Properties of propagation of electromagnetic wave in a multilayer radar-absorbing structure with plasma-and radar-absorbing material, *IEEE Transactions Plasma Science*, 39,9, pp. 1768–1775. (2011)
- [8] Mora P., Theoretical model of absorption of laser light by a plasma, *Phys. Fluids*, 25, 6, 1051. (1982)
- [9] Wang Y. and Zhou Z., “Propagation characters of Gaussian laser beams in collisionless plasma: Effect of plasma temperature,” *Physics of Plasmas*, 18, 4, 43101. (2011)
- [10] Muys P., Stimulated radiative laser cooling. *Laser Physics*, 18, 4, pp.430-433. (2008)
- [11] Djeu N. and Whitney W. T, Laser cooling by spontaneous anti-Stokes scattering. *Physical Review Letters*, 46, 4, 236. (1981)
- [12] Prince S. J., and Elder J. H., Probabilistic linear discriminant analysis for inferences about identity. In 2007 IEEE 11th International Conference on Computer Vision, pp. 1-8. (2007)
- [13] Jolliffe I. T., *Principal component analysis*. (2002)
- [14] Balakrishnama S. and Ganapathiraju A., Linear discriminant analysis-a brief tutorial. *Institute for Signal and Information Processing*, 18, 1-8. (1998)
- [15] Luthria D. L., Mukhopadhyay S., Robbins R. J., Finley J. W., Banuelos G. S., and Harnly J. M., “UV Spectral Fingerprinting and Analysis of Variance-Principal Component Analysis: a Useful Tool for Characterizing Sources of Variance in Plant Materials,” *J. Agric. Food Chem*, 56, 14, pp. 5457–5462. (2008)

[16] Paletou F., A critical evaluation of the principal component analysis detection of polarized signatures using real stellar data. *Astronomy & Astrophysics*, 544, A4. (2012)

[17] Larour J., et al, "Modeling of the L-shell copper X-pinch plasma produced by the compact generator of Ecole Polytechnique using pattern recognition." *Physics of Plasmas* 23.3, 033115. (2016)

[18] Tipping M. E. and Bishop C. M, Probabilistic principal component analysis. *Journal of the Royal Statistical Society: Series B (Statistical Methodology)*, 61, 3, pp.611-622. (1999)

[19] Ioffe S., Probabilistic linear discriminant analysis. In *European Conference on Computer Vision* Springer, Berlin, Heidelberg, 531-542. (2006)

[20] Simon Prince J.D. and Elder J. H, "Probabilistic linear discriminant analysis for inferences about identity." *IEEE 11th International Conference on Computer Vision*. (2007)

[21] Wiehr E., Spatial and temporal variation of circular Zeeman profiles in isolated solar Ca (+) K structures. *Astronomy and Astrophysics*, 149, 217-220. (1985)

[22] Goldstein T., Chen S., Tong Y., Xiao J., Ramasubramaniam A., and Yan, J., Raman scattering and anomalous Stokes–anti-Stokes ratio in MoTe 2 atomic layers. *Scientific reports*, 6, 28024. (2016)

[23] Da Silva M. L, Vacher D., André M. P., and Faure G., Radiation from an equilibrium CO<sub>2</sub>–N<sub>2</sub> plasma in the [250–850 nm] spectral region: II. Spectral modeling. *Plasma Sources Science and Technology*, 17, 3, 035013. (2008)

[24] Mahmoudian A., Scales, W. A., Bernhardt P. A., Briczinski S. J, and McCarrick M. J., Investigation of ionospheric stimulated Brillouin scatter generated at pump frequencies near electron gyroharmonics. *Radio Science*, 48, 6, 685-697. (2013)

[25] Yilmaz M. F, Danisman Y., Larour J. and Arantchouk L., Linear discriminant analysis, based predator-prey analysis of hot electron effects on the X-pinch plasma produced K-shell Aluminum spectra. *Scientific reports*, 9, 1, 1-8. (2019)

[26] Huba J. D, NRL plasma formulary. *NAVAL RESEARCH LAB WASHINGTON DC PLASMA PHYSICS DIV.* (2006)

[27] Leduc M., Julien D., and Juliette S., "Laser Cooling, Trapping, and Bose-Einstein Condensation of Atoms and Molecules." *AIP Conference Proceedings*, 1119, 1. (2009)

[28] Gorbachev V. S and Kel'Ner S. R, Plasma condensation formation in a fluctuating strong magnetic field. *Zh. Eksp. Teor. Fiz.*, 94, 89-99. (1988)

[29] O'Shea E., Banerjee D. and Doyle J. G, Plasma condensation in coronal loops. *Astronomy & Astrophysics*, 475, 2, L25-L28. (2007)

[30] Maximov A. V, Oppitz R. M, Rozmus W., and Tikhonchuk V. T, Nonlinear stimulated Brillouin scattering in inhomogeneous plasmas. *Physics of Plasmas*, 7, 10, 4227-4237. (2000)

[31] Watt R. G., Cobble J., DuBois D. F., Fernandez J. C., Rose H. A., Drake R. P., and Bauer B.S., Dependence of stimulated Brillouin scattering on focusing optic F-number in long scale-length plasmas. *Physics of Plasmas* 3,3 1091-1095 (1996).

[32] Rahman H. U, Shukla P. K, and A. C, Das, Excitation of convection cells by ion-cyclotron waves. *The Physics of Fluids*, 24, 10, 1802-1805. (1981)

[33] Stenzel R. L, Whistler waves with angular momentum in space and laboratory plasmas and their counterparts in free space. *Advances in Physics: X*, 1, 4, 687-710. (2016)

[34] McKenzie] J. F and Doyle T. B, Whistler oscillations and capillary-gravity generalized solitons. *Quaestiones Mathematicae*, 34, 3, 377-391. (2011)

[35] Rabinovich V. S, and Sanchez I. M., Radiation from non-uniformly moving sources in the plasma. In Proceedings of the International Seminar Days on Diffraction, 2004, IEEE, pp.163-174. (2004)

[36] Sprangle P., Esarey E., and Ting A, Nonlinear theory of intense laser-plasma interactions. *Physical Review Letters*, 64, 17. (1990)

[37] White R. B, Liu C. S., and Rosenbluth M. N., "Parametric decay of obliquely incident radiation." *Physical Review Letters* 31.8, 520. (1973)

[38] Gurnett D. A, et al, "Parametric interaction and spatial collapse of beam-driven Langmuir waves in the solar wind." *Journal of Geophysical Research: Space Physics* 86, A10 (8833-8841. 1981)

[39] W. Qin, Huang S., Du G., Zhang J., De G., Zhang J. and S. Lu, Anti-Stokes fluorescent cooling by energy transfer. *Journal of Luminescence*, 119, 356-360. (2006)

[40] Pugnet M., Collet J., and Cornet A., "Cooling of hot electron-hole plasmas in the presence of screened electron-phonon interactions." *Solid State Communications* 38, 6, 531-536(1981).